EARTH SURFACE PROCESSES AND LANDFORMS
Earth Surf. Process. Landforms **41**, 1564–1573 (2016)

Published online 25 April 2016 in Wiley Online Library
(wileyonlinelibrary.com) DOI: 10.1002/esp.3928

Observations of coastal cliff base waves, sand levels, and cliff top shaking

Adam P. Young,[1]* Robert T. Guza,[1] William C. O'Reilly,[1] Olivier Burvingt[2] and Reinhard E. Flick[1]
[1] Integrative Oceanography Division, Scripps Institution of Oceanography, University of California San Diego, La Jolla, CA, USA
[2] School of Marine Science and Engineering, Plymouth University, Plymouth, UK

Received 14 September 2015; Revised 28 January 2016; Accepted 16 February 2016

*Correspondence to: Adam P. Young, Integrative Oceanography Division, Scripps Institution of Oceanography, University of California San Diego, 9500 Gilman Dr., La Jolla, CA, 92093-0209, USA. E-mail: adyoung@ucsd.edu

ESPL
Earth Surface Processes and Landforms

ABSTRACT: Concurrent observations of waves at the base of a southern California coastal cliff and seismic cliff motion were used to explore wave–cliff interaction and test proxies for wave forcing on coastal cliffs. Time series of waves and sand levels at the cliff base were extracted from pressure sensor observations programmatically and used to compute various wave impact metrics (e.g. significant cliff base wave height). Wave–cliff interaction was controlled by tide, incident waves, and beach sand levels, and varied from low tides with no wave–cliff impacts, to high tides with continuous wave–cliff interaction. Observed cliff base wave heights differed from standard Normal and Rayleigh distributions. Cliff base wave spectra levels were elevated at sea swell and infragravity frequencies. Coastal cliff top response to wave impacts was characterized using microseismic shaking in a frequency band (20–45 Hz) sensitive to wave breaking and cliff impacts. Response in the 20–45 Hz band was well correlated with wave–cliff impact metrics including cliff base significant wave height and hourly maximum water depth at the cliff base ($r^2 = 0.75$). With site-specific calibration relating wave impacts and shaking, and acceptable anthropogenic (traffic) noise levels, cliff top seismic observations are a viable proxy for cliff base wave conditions. The methods presented here are applicable to other coastal settings and can provide coastal managers with real time coastal conditions. Copyright © 2016 John Wiley & Sons, Ltd.

KEYWORDS: coastal cliff; wave–cliff interaction; wave impact; cliff shaking; microseismic

Introduction

Wave erosion is a fundamental process of coastal cliff morphology yet field studies of wave–cliff interaction are rare. Observations of cliff base waves (i.e. Stephenson and Kirk, 2000; Young *et al.*, 2011a; Dickson and Pentney, 2012) and sand levels (Robinson, 1977), and the corresponding cliff erosion rate, are lacking (Naylor *et al.*, 2010; Sunamura, 2015). Unvalidated parameterizations of marine forcing and cliff response are therefore necessarily used in model simulations and studies of past and future cliff erosion (e.g. Sunamura, 1982; Budetta *et al.*, 2000; Young *et al.*, 2009; Revell *et al.*, 2011; Castedo *et al.*, 2012; Hackney *et al.*, 2013). Here, concurrent field observations of cliff top shaking, and waves and sand levels at a cliff base, are used to compare metrics of wave–cliff interaction, and to explore recent suggestions that seismic cliff top observations (at particular frequencies) provide a useful proxy for wave impacts on a cliff. Automated methods to extract time series of beach elevation and wave heights from a buried pressure sensor are also presented.

Background

Methods to characterize the potential of waves to cause coastal erosion incorporate a variety of measured and estimated wave characteristics.

Wave impact forces

Wave-impact pressures vary widely depending on the type of wave–cliff interaction, generally classified as broken (bore) impacts, breaking impacts (waves breaking into the cliff), and reflective. Oumeraci *et al.* (1993) further divided breaking impact types into three categories based on air entrapment. Impulsive and pulsating wave loads are both observed on coastal structures. Many existing empirical and theoretical equations of wave loads on cliffs and seawalls depend on the wave height at the cliff base (H_{Cliff}) and bore speed (C). Example force (F) estimates are:

$$F = A\rho g H_{\mathrm{Cliff}} \tag{1}$$

where A, ρ, and g are a calibration constant, water density, and gravitational acceleration, respectively (Sunamura, 1977).

$$F = 4.5\rho g H_{\mathrm{Cliff}}^2 \tag{2}$$

(Camfield [1991] after Cross [1967] broken wave force).

$$F = 0.5\rho C^2 H_{\mathrm{Cliff}} \tag{3}$$

(Larson *et al.* [2004] swash bore force).

$$F = 4.76\rho g H^2_{\text{Cliff-Sig}} \quad (4)$$

(Cuomo *et al.* [2010] quasi-static load).

$$F = F^*\rho g H^2_{\text{Cliff-Sig}} \quad (5)$$

(Oumeraci *et al.* [2001] maximum impulse force) where F^* is the relative maximum wave force, assumed to follow a Generalized Extreme Value distribution. Blackmore and Hewson (1984) found average pressures from broken waves of:

$$P = \lambda\rho T C^2 \quad (6)$$

where λ is aeration factor, and T is wave period.

Wave–cliff interaction proxies

Simple proxies for marine forcing at coastal cliffs include incident wave height, energy (Davidson-Arnott and Ollerhead, 1995), and power (Kamphuis, 1987; Brown *et al.*, 2005). These proxies neglect local influences such as shoaling, dissipation, runup, and beach elevation (although they are sometimes site-calibrated to incorporate local influences). Some studies include site conditions using a total water level (TWL) method, where TWL is the sum of tides and the vertical height of wave setup and runup (Shih *et al.*, 1994; Kirk *et al.*, 2000; Ruggiero *et al.*, 2001). When TWL exceeds the cliff base beach elevation, wave–cliff impact occurs. The duration of wave attack provides an indicator of marine forcing (Ruggiero *et al.*, 2001; Sallenger *et al.*, 2002) and has been used in previous cliff studies (i.e. Young *et al.*, 2009, 2011b; Young, 2015). However, detailed beach elevation data are often unavailable and if lacking, Collins and Sitar (2008) suggested using maximum daily TWL relative to seasonal elevation averages.

Methods neglecting cliff base beach elevations as an important factor are clearly insufficient (when beaches are present). At the other extreme, models that only consider wave impact duration neglect the relative amount of energy available for potential marine-driven erosion. Brown *et al.* (2005) and Swenson *et al.* (2006) derived marine-forcing proxies that include wave impact height using the cliff base water depth defined as the difference between TWL and cliff base beach elevation. TWL methods are based on maximum runup and neglect the distribution of wave impact heights. Hughes *et al.* (2010) explored wave runup distributions on a sandy coast, but there have been no similar studies on cliffed coasts. Lacking cliff base wave observations, Wilcock *et al.* (1998) developed a frequency distribution of impact wave height from synthetic wave records transformed across the nearshore to estimate wave–cliff impact pressures and a proxy for wave–cliff interaction.

Other studies have included the influence of site conditions indirectly. Amin and Davidson-Arnott (1997) used incident wave energy as the marine-forcing proxy but also included sediment availability, cliff height, and potential longshore transport using a multi-variable regression. Benumof *et al.* (2000) defined a proxy of 'wave power at the cliff' as wave power multiplied by vertical runup and suggested that because slope is included in the runup calculation, local site conditions are inherently addressed. Kline *et al.* (2014) developed a numerical cliff retreat model using wave forcing established from wave impact height modified by beach elevation and water level. Trenhaile (2000) included local site effects and developed a proxy from breaker height, surfzone width, type of breaking waves, and roughness of the rock surface. Sunamura (1982), Wilcock *et al.* (1998), and Trenhaile (2000) also suggest using a threshold-based metric where a minimum site specific value is necessary to cause erosion.

Microseismic cliff motions

Seismic observations at coastal cliffs suggest ground motions generated by local ocean waves may provide a convenient proxy for wave–cliff impacts (long-term logistics for a cliff top seismometer are often easier than for a cliff base pressure sensor). Cliff ground motions are driven by different local mechanisms in two general frequency bands. Low-frequency cliff motion (0.01–0.1 Hz) or 'flexing' is generated by individual sea, swell (Adams *et al.*, 2005), or infragravity (Young *et al.*, 2011a, 2012, 2013) waves that load the foreshore with pressure fluctuations and exert gravitational attraction (Agnew and Berger, 1978). Double frequency (DF) motions are non-locally generated and propagate trans-continental distances (e.g. Bromirski, 2001). Higher frequency cliff motion (HF, $>$ 0.3 Hz) or 'shaking' is generated from ocean waves directly impacting the cliff (Adams *et al.*, 2002) or fronting shore platforms (Dickson and Pentney, 2012), wind (Norman *et al.*, 2013), waves breaking in the nearshore (Young *et al.*, 2013; Poppeliers and Mallinson, 2015), and anthropogenic sources such as vehicle traffic. These various contributions to HF shaking frequencies complicate the isolation of seismic signals from wave–cliff impacts. Peaks at various frequencies in HF energies have been observed at several sites (Dickson and Pentney, 2012; Young *et al.*, 2013) and are possibly related to site conditions, geometry, and geologic composition.

Lim *et al.* (2011) attributed cliff shaking ($<$300 Hz) to wave–cliff impacts and found distinct water levels were associated with an elevated cliff response. Norman *et al.* (2013) observed elevated cliff shaking signals (1.1–50 Hz) only during combined elevated water levels and waves. Norman *et al.* (2013) and Vann Jones *et al.* (2015) selected shaking at 9.6 Hz to represent wave–cliff interaction because it experiences the highest amplitudes without overlapping other shaking signals (i.e. wind generated). Vann Jones *et al.* (2015) found cliff shaking (9.6 Hz) correlated (multiple regression, $R^2 = 0.53$) with modeled cliff base wave height (includes the influence of tide) and wave setup, supporting the use of cliff motion as a proxy for wave–cliff impacts. Previous studies lack quantitative analysis of concurrent observations of cliff base waves and cliff shaking. Here, pressure sensor observations at the base of a coastal cliff are used to determine the heights and frequency of wave–cliff impacts, and to measure cliff base beach elevations. Observations of cliff ground motions are examined in the context of the wave observations and associated metrics of wave–cliff interaction.

Study Site

Cliff setting

The studied 24 m high cliff, located in northern Del Mar, California, USA, consists of three geologic units (Figure 1). The lower unit is the Del Mar Formation, an Eocene sedimentary deposit composed of sandy claystone interbedded with coarse-grained sandstone, overlain conformably by Torrey Sandstone, a massive coarse-grained and well cemented Eocene sandstone (Kennedy, 1975). Together, these two units form the lower near-vertical portion of the cliff up an elevation of about 8 m (navd88). The upper cliff section is about 16 m thick, slopes at 35°–50° and consists of weakly cemented, fine-grained sandy Pleistocene terrace deposits. The contact

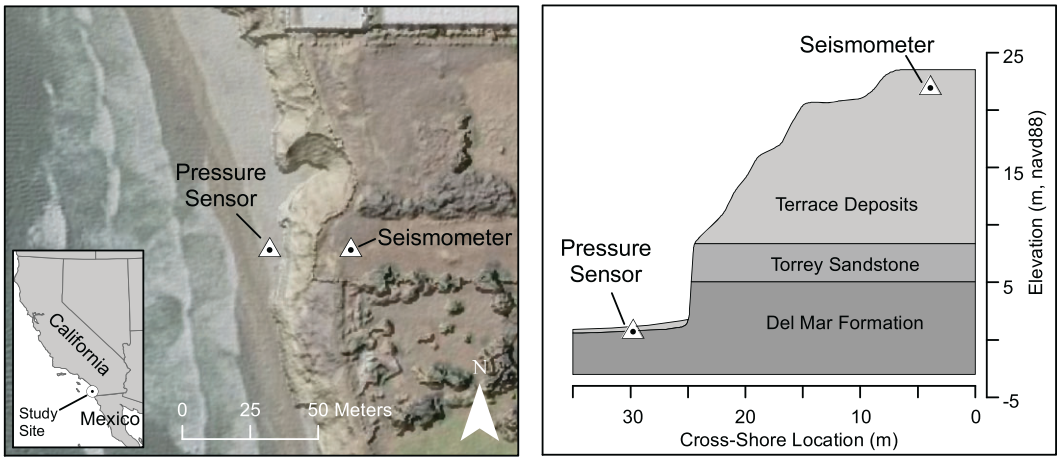

Figure 1. (left) Cliff study site, location map and (right) cliff profile, geology, and instrumentation.

between the Del Mar and Torrey Sandstone Formations decreases in elevation toward the north and terminates abruptly at a fault immediately north of the instrumentation setup. The lower Eocene units are harder and more resistant to erosion compared to the softer marine terrace deposits. Typical cohesion and friction angle values for undisturbed Del Mar Formation and Terrace Deposits are 31 kPa, 47°, and 14 kPa, 36°, respectively (Leighton and Associates, 2003). The cliff is fronted by a narrow dissipative sand (and occasionally cobble) beach, which is often submerged during high tides. The underlying shore platform composed of the Eocene units is gently sloping and relatively smooth near the shoreline, and more irregular offshore, forming nearshore reefs. The shore platform elevation at the cliff base is close to mean lower low water (about 1 m navd88). Sand thickness at the cliff base is typically several meters, but is occasionally reduced to zero when winter storm waves expose the shore platform. The shore platform extends alongshore 0.4 km southward and 2.4 km northward. Offshore the platform contains transient sand pockets and plants.

Oceanographic setting

The cliffs are exposed to waves generated by local winds and distant storms in both hemispheres. During winter, swell from the North Pacific and Gulf of Alaska is most energetic, whereas swell from the South Pacific dominates in summer. Waves reaching southern California cliffs undergo a complex transformation, and 'shadows' of the Channel Islands create strong alongshore variations in wave height (e.g. Pawka, 1983). The seasonal cycle in the Del Mar region has maximum wave energy in winter. The tide range is approximately 2 m (http://tidesandcurrents.noaa.gov).

Methods

Incident waves

A wave buoy network (CDIP, http://cdip.ucsd.edu) was used to estimate hourly significant wave height ($H_{10\text{-Sig}}$, Figure 2a) and peak period (T_p) at a virtual buoy seaward of the study area in 10 m water depth. The effects of complex bathymetry in the southern California Bight, and of varying beach orientation and wave exposure, were simulated with a spectral refraction wave model initialized with offshore buoy data (O'Reilly and Guza, 1991, 1993, 1998).

Tides (offshore water level)

Hourly water levels seaward of the surfzone (h_{wl}), including tides, atmospheric pressure and wind effects, were obtained from the La Jolla tide gauge #94101230 (http://tidesandcurrents.noaa.gov), located in about 7 m water depth 12 km south of the study site.

Modeled total water level (TWL)

The modeled hourly TWL is the sum of offshore water levels and vertical runup

$$\mathrm{TWL} = h_{wl} + R_{2\%} \tag{7}$$

where $R_{2\%}$, is the level exceeded by 2% of wave uprushes,

$$R_{2\%} = 1.1\left\{0.35\beta_f(H_oL_o)^{0.5} + \left(\left[H_oL_o\left(0.563\beta_f^2 + 0.004\right)\right]^{0.5}\right)/2\right\} \tag{8}$$

where H_o and L_o characterize the incident deep water wave height and wavelength, respectively (Stockdon *et al.*, 2006). The value of H_o was calculated by backing out H_{10} to deep water by reverse shoaling using linear wave theory, while L_o was calculated using the deep water linear dispersion relationship and the peak period. The beach slope (β_f) was estimated as the mean slope of a 20 m horizontal swath centered on the intersection of hourly mean sea level and interpolated beach profile from four ATV-GPS (all terrain vehicle equipped with differential global positioning system) surveys (conducted on October 11, 2010, November 8, 2010, December 17, 2010, and January 4, 2011).

Cliff base pressure sensor

A Paroscientific pressure sensor (model# 245A-102), sampling at 8 Hz from November 4, 2010 to December 20, 2010, was located on the shore platform (1.02 m elevation, datum-NAVD88) approximately 4 m shoreward of the cliff base. Atmospheric pressure was removed from the record using linearly interpolated six-minute observations collected approximately 12 km south of the study site on a pier.

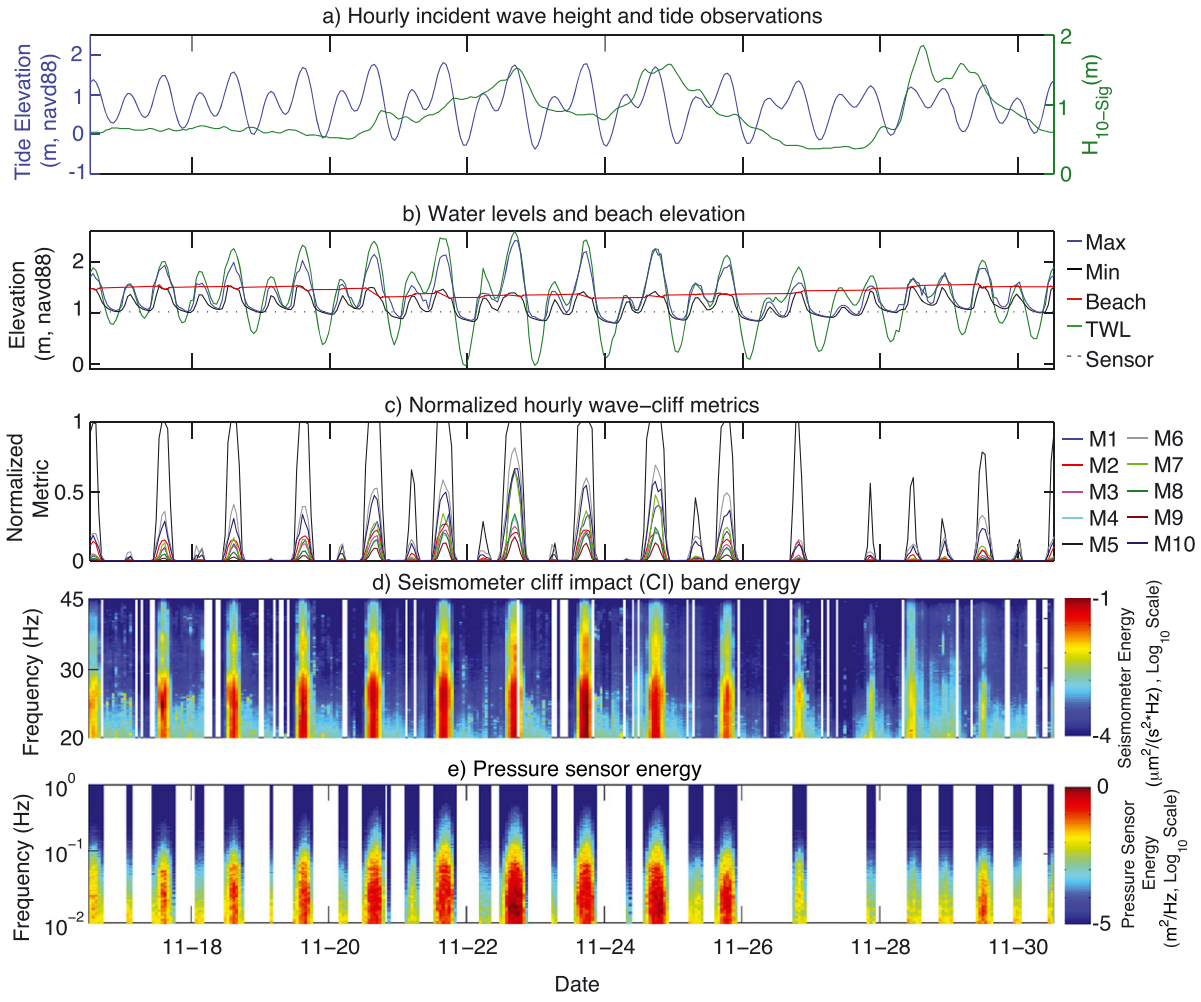

Figure 2. Two weeks of hourly (a) observed tide elevation and modeled incident significant wave height in 10 m water depth $H_{10\text{-sig}}$, (b) observed hourly maximum and minimum observed water level, modeled total water level (TWL), cliff base beach elevation, and pressure sensor elevation, (c) normalized hourly wave–cliff interaction metrics, (d) cliff top seismometer vertical velocity spectra (color bar) and (e) cliff base water level spectra (color bar). In (e), white bands corresponds to time periods with no wave–cliff interaction.

Pressure time series were corrected for clock drift and converted to hydrostatic elevation relative to NAVD88.

Automated beach elevation extraction

After a wave recedes, the fully saturated subaerial beach can be exposed, and the water level is relatively constant for several seconds (Figure 3b, Raubenheimer *et al.*, 1995). Beach elevations were detected by locating points in the time series with slope (running mean over a 10 second window) near zero, 25–35 seconds after a wave crest passes (red dots in Figures 3b and 3c). Multiple points identified between successive waves were reduced to a single representative beach elevation, yielding 3269 values, generally at the beginning and end of the high tide cycles. Beach elevations from the pressure sensor were consistent with ATV-GPS beach surveys on November 8, 2010 and December 17, 2010.

Automated wave height estimation

Discontinuous wave time series at the cliff base precluded using typical zero-crossing wave detection methods. Instead, wave peaks and troughs were detected programmatically using consecutive local minima and maxima (similar to the methods of Hughes *et al.*, 2010) and a minimum wave height threshold of 1 cm. When the interval between waves was long enough, drainage from the beach (Figure 3c) generated local water level minima unrelated to waves at the cliff base. These subsurface minima were programmatically excluded from wave height estimates.

Wave–cliff interaction metrics

Cliff base wave heights (H_{Cliff}) and water levels from the pressure sensor observations (water levels include tide, wave height, setup, etc.) were used to calculate the following observed hourly wave–cliff interaction metrics (Figure 2c):

M1: Variance of cliff base water level (about the mean, water table fluctuations removed)
M2: Number of cliff base waves (N)
M3: Sum of cliff base wave heights ($\Sigma\ H_{Cliff}$)
M4: Sum of squared cliff base wave heights ($\Sigma\ H^2_{Cliff}$)
M5: Duration of wave attack (fraction during each hour)
M6: Significant cliff base wave height ($H_{Cliff\text{-}Sig}$, average of 1/3 highest H_{Cliff})
M7: Significant cliff base wave height squared ($H^2_{Cliff\text{-}Sig}$)
M8: $H^2_{Cliff\text{-}Sig}$ * N (M8 = M7*M2)
M9: Swash wave force (Equation 3, Larson *et al.*, 2004) where wave speed is:

$$C = (g^*(\text{wave peak elevation} - \text{beach elevation}))^{0.5} \quad (9)$$

M10: Maximum instantaneous water depth (maximum water elevation – beach elevation)

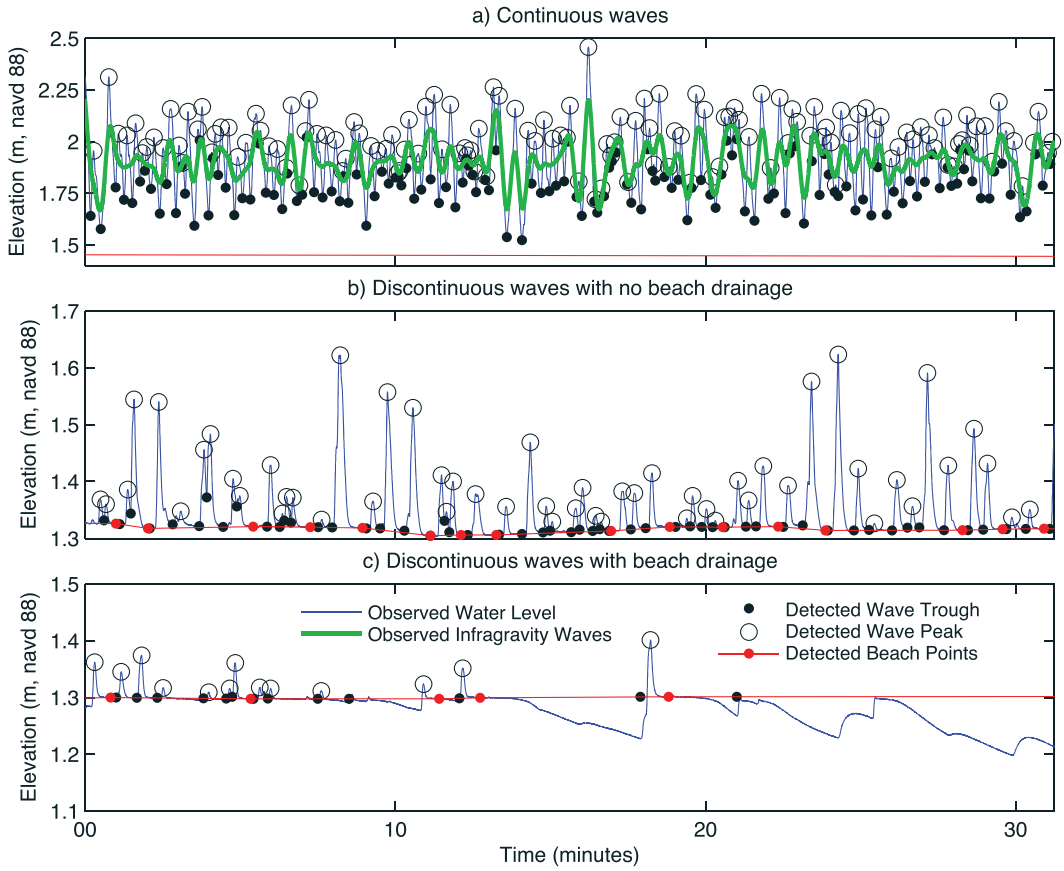

Figure 3. Observed water level versus time (blue curve) with detected wave peaks, troughs and beach elevations for time periods of (a) continuous cliff base waves, (b) discontinuous waves and fully saturated beach between waves, and (c) discontinuous waves and water levels draining below beach elevation. In (a), much of the variance is at infragravity frequencies (green curve).

Cliff top ground motions

Ground motions were measured at 100 Hz with a Nanometrics Compact Trillium broadband seismometer near the cliff top edge (elevation 23.5 m, NAVD88), 26 m shoreward of the pressure sensor. The raw vertical velocity data were phase and magnitude corrected in the frequency domain according to the instrument response curve. Seismic and cliff base water levels, divided into one hour records, were processed with standard Fourier spectral and cross-spectral methods (Jenkins and Watts, 1968). Hours containing significant ground motion from earthquakes, post-installation settlement, or local noise were removed manually. Spectral seismic data was used to identify both useful wave–cliff interaction metrics and the specific seismic frequency range (20–45 Hz) suited for impact detection. All correlations presented are statistically significant ($p << 0.05$).

Observations

General conditions

Incident wave heights (H_{10}) ranged from 0.36 to 1.84 m (average 0.83 m, Figure 2a). The observed water level exceeded the cliff base beach elevation during 46% of the study period (513 of 1123 hours). Continuous wave–cliff interaction occurred for 89 hours, during the highest tides. Hours with discontinuous wave–cliff interaction occurred more frequently (424 hours), usually before and after high tides, but also occasionally during entire high tide cycles. Waves did not reach the cliff during low tide. Beach elevations at the cliff base fluctuated about 0.59 m over the study period (1.03–1.62 m, NAVD88), with a maximum change of 26 cm over a single high tide cycle. Negative pressures, yielding observed water levels as much as 20 cm below the sensor (Figure 2b) are likely associated with the capillary fringe (Cartwright *et al.*, 2006).

Cliff seismic motions generally increased with increasing tide and incident wave energy, consistent with previous studies. Cliff shaking energies, wave impact metrics, and pressure sensor energies are all tidally modulated (Figures 2c–2e). Spectra of cliff top vertical ground velocity are most energetic at infragravity and single frequencies. The HF shaking band has peaks at about 1 and 7 Hz (Figure 4b).

Total water level (TWL)

Modeled TWL ranged from about 1.5 m above to 1.5 m below the cliff base sand level (green relative to red curves in Figure 2b). Modeled TWL generally agreed well with observed maximum water elevation at the cliff base (M10) for hours with observed wave–cliff interaction ($r^2 = 0.81$, Figure 2b). Some offset (about 10 cm in Figure 2b) is expected, given the substantial scatter in the underlying Stockdon *et al.* (2006) parameterization (Equation 8). Overall, TWL provides reasonable estimates of the observed maximum cliff base water level when compared to the extracted beach elevations, correctly determining hours with wave–cliff impacts 90% of the time. However without consideration of beach elevation, TWL alone is not a direct measure of wave–cliff interaction because sand levels influence whether wave–cliff interaction occurs.

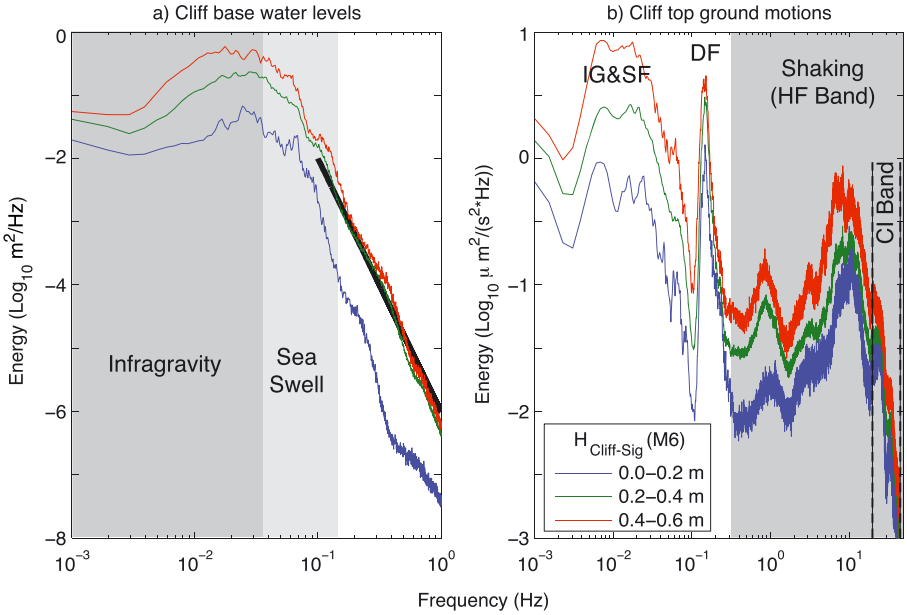

Figure 4. Frequency (f) spectra of (a) cliff base water level (black line has f^{-4} dependence) and (b) cliff top vertical ground velocity when the cliff base is always covered with water (e.g. continuous waves, Figure 2a). Note the axes vary between panels. Spectra are averaged over cases with three ranges of significant wave height at the cliff toe (M6, legend). The infragravity and sea-swell frequency bands are indicated in (a), and combined (IG & SF) in (b). In (b), the high frequency (HF, gray) shaking band contains the wave–cliff impact sub-band (CI, dashed lines). DF is the remotely generated, double frequency band.

Observed cliff base wave heights

Cliff base wave heights ranged up to 1.17 m with mean and standard deviation both equal to 0.13 m. Binned (0.05 m bin size) hourly wave height distributions (hours with at least 100 waves) were consistently skewed with relatively more small waves than a Rayleigh distribution and often peaked in the minimum bin (0–0.05 m, Figure 5a). Wave heights increase with hourly maximum cliff base water depth (M10), causing an increase in the cumulative hourly wave height distribution and a wider range of wave heights (Figure 6). The ensemble-average of the measured probability distribution differs from both standard Rayleigh and Normal distributions often used to describe offshore wave heights (Figure 5).

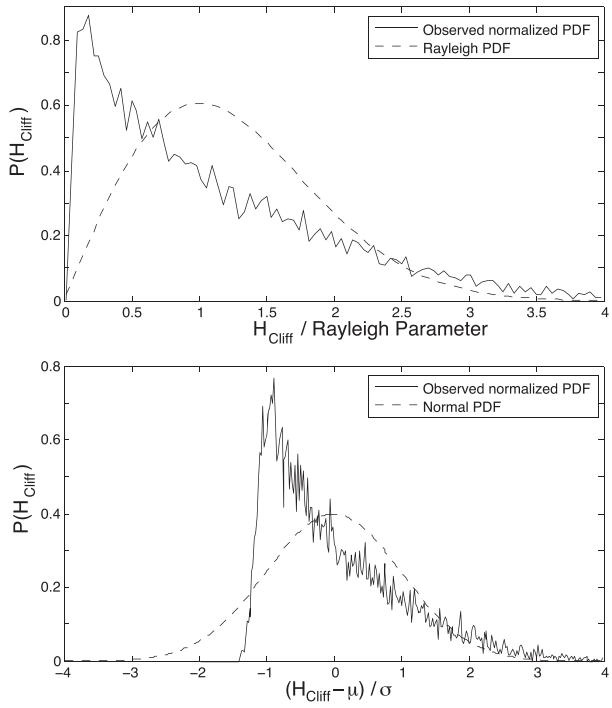

Figure 5. Normalized ensemble-average observed cliff base wave (H_{Cliff}) distribution (for hours with at least 100 waves used) compared with standard (top) Rayleigh and (bottom) Normal distributions.

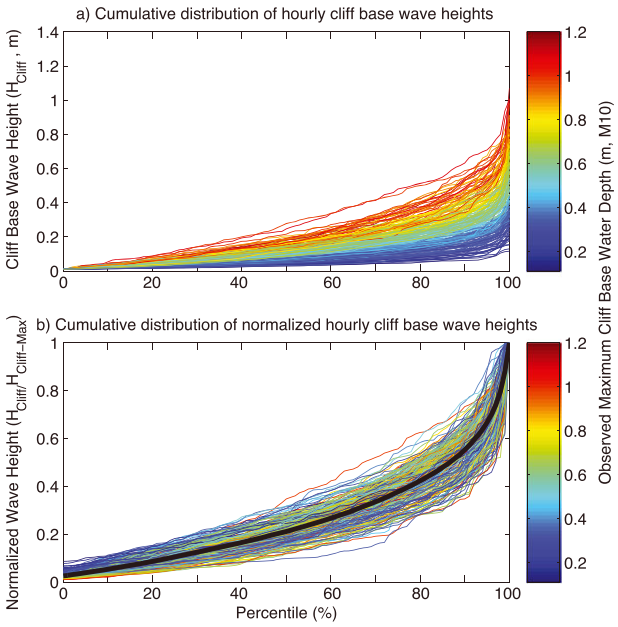

Figure 6. Cumulative distribution of (a) cliff base impact wave heights (H_{Cliff}) during each hour, and (b) cliff base impact wave heights normalized by maximum hourly cliff base wave height ($H_{Cliff\text{-}Max}$) during each hour and the overall mean (thick black line). Colors are observed maximum hourly cliff base water depth (M10).

Observed cliff base wave spectra

Hourly cliff base wave energy spectra generally increased with tide and cliff base water depth (Figure 2e). Spectra levels increased with wave period and exhibited high infragravity energies (Figure 4a), consistent with recent research highlighting the importance of infragravity waves in rock coast processes

(Beetham and Kench, 2011; Young *et al.*, 2011a, 2012, 2013, Ogawa, 2012; Dickson *et al.*, 2013; Earlie *et al.*, 2015). Energy spectra at sea-swell frequencies (f) and higher decrease as f^{-4} (Figure 4a).

Observed wave-impact metrics

All impact metrics (Figure 2c) were tidally modulated and usually mutually correlated (Table I; mean $r^2 = 0.68$, median $r^2 = 0.71$). M5 was the least correlated overall (r^2 between 0.21–0.8, mean 0.50), while M1, M3, M4, and M8 were best correlated (mean $r^2 \sim 0.75$). For a Rayleigh wave height distribution M4 and M8 are linearly correlated ($r^2 = 1$, M8 = 2*M4). Deviations from the Rayleigh distribution alter the observed proportionality to M8 ~ 2.2*M4. During periods of intermittent swash (when the wave trough was equivalent to beach elevation) M9 and M4 differ only by a constant because squared bore speed is proportional to wave height (H_{Cliff}), and $r^2 = 1$. When waves are continuous, bore wave speed (Equation 9) included the variable depth below the wave trough and is not proportional to wave height (H_{Cliff}), causing a deviation between M9 and M4. However the deviation only causes a slight decrease in correlation and correlations between M9, M4, and similarly M8 are high (r^2 ranges from 0.92 to 1.00).

Discussion

Correlation of wave impact metrics with shaking

Impact metrics show higher correlations (Figure 7) with seismic energy at cliff impact frequencies (20–45 Hz). Cliff impact energy has the highest correlation $r^2 > 0.7$ with impact metrics M5, M6, and M10 (Figure 7, Table I). Metrics related to ΣH_{Cliff}^2 (M4, M8, and M9) are least correlated with cliff impact energy ($r^2 = 0.34$–0.48). The 9.6 Hz wave impact band of Vann Jones *et al.* (2015) is not correlated with any metrics (Figure 7), suggesting site conditions influence cliff impact seismic response consistent with previous research (Dickson and Pentney, 2012; Young *et al.*, 2013). Correlations are elevated slightly ($r^2 \sim 0.3$) around 1 Hz and 7 Hz, corresponding to peaks in the cliff top HF energy spectra (Figure 4b). Cliff impact energy levels are much lower than these peak HF frequencies (Figure 4b), but the r^2 of cliff impact with impact metrics is much higher (Figure 7).

Effect of conditions on wave impacts

The ability of waves to interact with the cliff is largely controlled by the difference between tide (observed) and beach elevation (M10 is shown in Figure 8a). All metrics except M6 and M7 were maximum during two consecutive hours with

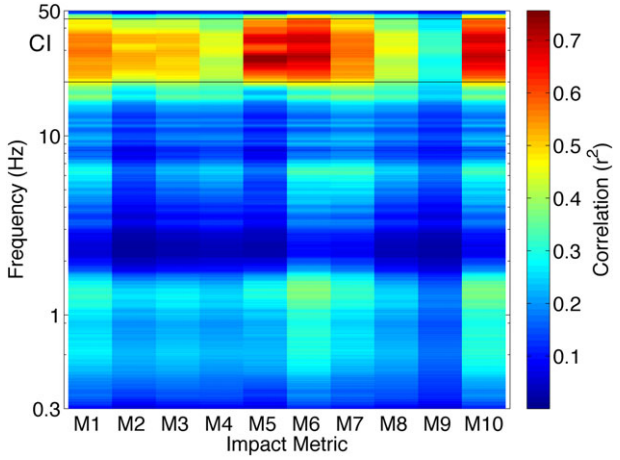

Figure 7. Correlation (r^2, color bar) between each of 10 wave impact metrics (horizontal axis) and cliff top high frequency seismic energy versus frequency (vertical axis). The highest r^2 (>0.7) is in the cliff impact band (CI, 20–45 Hz), for metrics M5, M6, and M10.

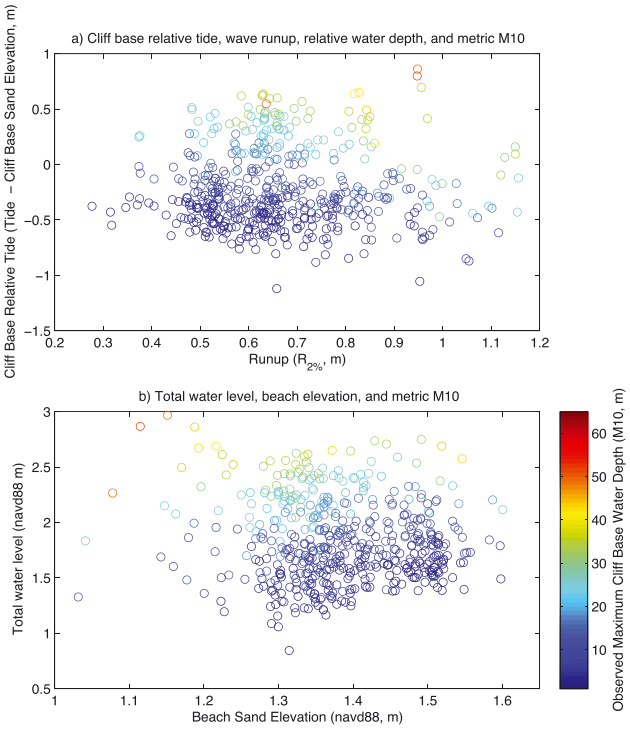

Figure 8. Impact metric M10 (observed maximum depth at cliff base, color bar) versus (horizontal and vertical axes, respectively) (a) cliff base relative tide (tide level minus beach elevation) and wave-induced runup, (b) modeled total water level and beach sand elevation. Only hours with M10 > 0 are shown.

Table I. The r^2 correlation matrix of wave–cliff impact metrics and cliff impact shaking (CI, 20–45 Hz)

	M1	M2	M3	M4	M5	M6	M7	M8	M9	M10	CI
M1	1.00	0.69	0.83	0.84	0.51	0.78	0.87	0.85	0.65	0.85	0.61
M2		1.00	0.91	0.75	0.57	0.53	0.43	0.74	0.71	0.72	0.56
M3			1.00	0.95	0.45	0.57	0.57	0.94	0.90	0.75	0.56
M4				1.00	0.34	0.54	0.63	1.00	0.93	0.69	0.48
M5					1.00	0.80	0.54	0.34	0.21	0.77	0.73
M6						1.00	0.87	0.54	0.34	0.93	0.75
M7							1.00	0.64	0.39	0.81	0.63
M8								1.00	0.92	0.69	0.48
M9									1.00	0.51	0.34
M10										1.00	0.75

elevated tide, moderate waves (H_{10} = 1.17 m), and near minimum beach sand elevations (1.08 m NAVD88, Figure 8b). At the same tide level, small waves with depleted beaches can cause more cliff shaking than larger waves with an elevated beach.

Cliff shaking as a wave impact proxy

Infragravity (IG) signals increase approximately linearly with cliff base water depth (TWL, Figure 9a), consistent with forcing by nearshore loading and gravitational attraction. Cliff impact ground motions trend consistently only during hours of wave–cliff interaction (cliff base depths > 0, Figure 9b). During hours without wave–cliff interaction, traffic noise may contribute to the scattered seismometer energy between $10^{-3.5}$ and 10^{-4}, independent of cliff base water depth. Traffic noise may contaminate shaking band signals at this and other sites.

Elevated cliff impact signals during periods of wave–cliff interaction and good correlations between cliff impact energy and several cliff base wave metrics suggest that cliff motions probably provide a proxy for wave–cliff impacts at certain site-specific frequencies. However, bursts of elevated cliff top ground motion were not always coincident with peaks in cliff base water levels (Figure 10), possibly because the seismometer responds to wave breaking displaced alongshore from the seismometer. The spatial range of detectable wave–cliff impacts is unknown. Similarly, wave breaking on the beach fronting the cliff excites ground motion at the seismometer, as observed at other sites (e.g. Young *et al.*, 2013). Detailed observations of wave breaking and cliff impacts in space and time are needed to link individual wave characteristics to cliff shaking. More studies of concurrent quantitative cliff base wave observations, video monitoring, and coastal and inland seismic motion are needed to reduce uncertainties associated with the generation of coastal seismic motions. Long-term observations are needed to link cliff erosion with wave impacts and/or shaking.

Modeling and monitoring applications

Lacking cliff base wave observations, maximum hourly water depth (M10) can be modeled using beach slope and elevation,

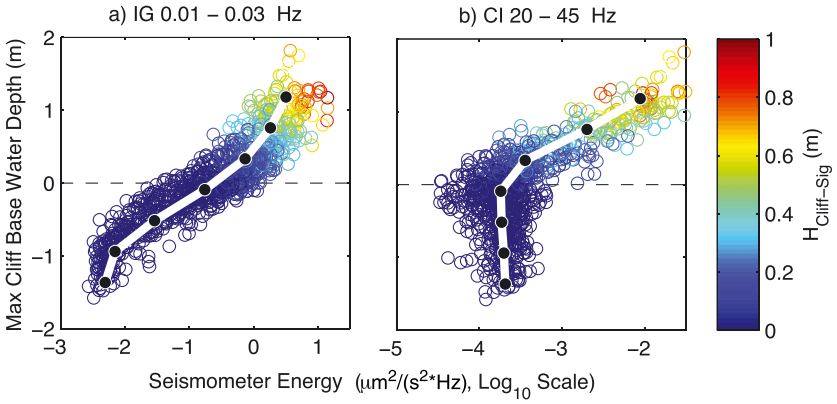

Figure 9. (a) Infragravity (IG, 0.01–0.03 Hz) band and (b) cliff impact band (CI, 20–45 Hz) seismic energy density versus modeled maximum hourly cliff base water depth (modeled TWL − observed beach elevation). Colors correspond to hourly significant wave height at the cliff base $H_{\text{Cliff-Sig}}$ (M6). Mean binned data are black dots and white lines. (b) When (TWL − beach elevation) < 0 (dashed horizontal line) there is no wave–cliff interaction, the cliff impact band does not depend on (TWL − beach elevation), and may be dominated by traffic or other noise. Modeled cliff base water depth was used to expand the plot and include negative cliff base water depths.

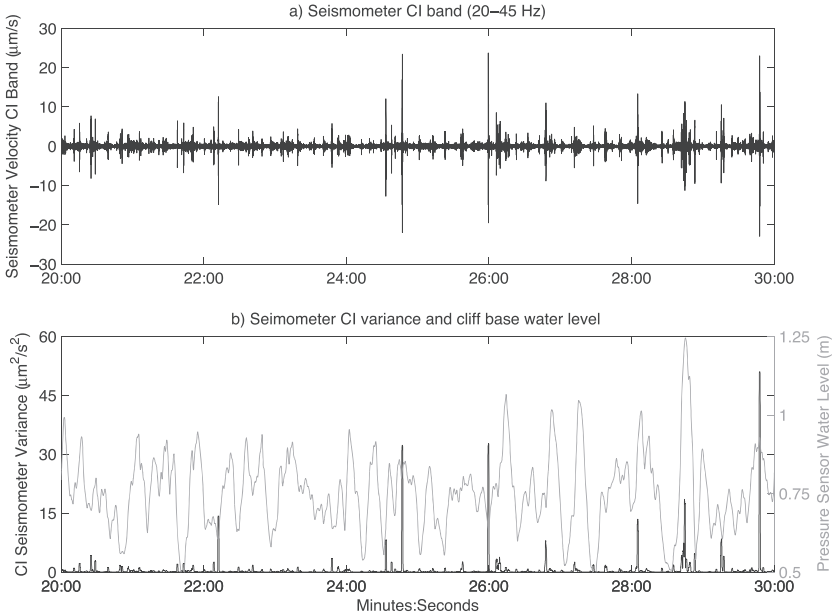

Figure 10. (a) Vertical velocity in the cliff impact (CI, 20–45 Hz) band versus time for 10 minutes. (b) Seismic vertical velocity variance in a sliding one second window (left axis) and observed cliff base water elevation (right axis) versus time. Bursts of cliff impact energy are not obviously associated with waves that are particularly large, or with wave crests.

wave models and empirical formulae for runup (for example the TWL method used here). M10 correlates very well ($r^2 = 0.97$) with observed maximum hourly cliff base wave height and can be used to generate synthetic time series of cliff base waves from the normalized wave height distribution (Figure 6b). Modeled M10 is a convenient measure of marine forcing in cliff models for this site, in lieu of wave impact and seismic observations. M10 is similar to the wave impact metric (modeled cliff base wave height plus wave setup) that Vann Jones *et al.* (2015) found best correlated with cliff shaking, suggesting M10 could be applicable at other sites and used to improve rock coast models (e.g.Trenhaile, 2011; Limber *et al.*, 2014).

This study describes two methods to monitor wave–cliff interaction and nearshore conditions. A cliff base pressure sensor was used to observe waves, water levels, and beach sand levels at one location. The sand level observations derived from the pressure sensor require less labor than repeated GPS field surveys, and provide high temporal resolution data. Seismic observations can provide a proxy for nearshore conditions and wave–cliff impacts, and can survive storm conditions when *in situ* instrumentation may fail. Both methods can provide coastal managers with real-time quantitative coastal conditions and contribute new approaches to the growing research on rock coast processes (Naylor *et al.*, 2014).

Summary

Wave heights and beach elevations, programmatically extracted from cliff base pressure sensor observations, are used to explore wave–cliff interaction and develop wave–cliff impact metrics. Spectra of cliff base water levels were elevated at sea swell and infragravity energies. Cliff shaking signals between 20–45 Hz were above noise levels only during periods of wave–cliff interaction and correlate well with several wave–cliff impact metrics. Cliff motions at site specific frequencies appear to provide a proxy for wave–cliff interaction. Impact metrics of hourly cliff base significant wave height, maximum cliff base water depth, and duration of wave attack were best correlated with cliff shaking ($r^2 = 0.73$–0.75). Maximum hourly cliff base water depth provides a robust wave-based metric for marine forcing and can be modeled with runup equations and beach elevations. Cliff shaking frequencies most correlated with cliff base wave metrics differed from peak frequencies in the seismic signals that are generated by incident wave loading and distant ocean waves. The methods presented here are applicable to a wide range of settings beyond rock coasts, and can provide novel real-time time series of beach sand levels and hydrodynamic conditions.

Acknowledgements—APY was funded by the California Department of Parks and Recreation, Division of Boating and Waterways (DPR-DBW) with the University of California. RTG was supported by the US Army Corps of Engineers. Wave data collection was sponsored by the DPR-DBW and USACOE, as part of the Coastal Data Information Program. Engineer Brian Woodward and staff collected the pressure observations. The authors thank the Del Mar Beach Club, the Solana Beach Lifeguards, and the Jacobs family for their assistance.

References

Adams PN, Anderson RS, Revenaugh J. 2002. Microseismic measurement of wave-energy delivery to a rocky coast. *Geology* **30**(10): 895–898.

Adams PN, Storlazzi CD, Anderson RS. 2005. Nearshore wave-induced cyclical flexing of sea cliffs. *Journal of Geophysical Research, Earth Surface* **110**(F2): F02002.

Agnew DC, Berger J. 1978. Vertical seismic noise at very low frequencies. *Journal of Geophysical Research, Solid Earth* **83**(B11): 5420–5424.

Amin SMN, Davidson-Arnott RG. 1997. A statistical analysis of the controls on shoreline erosion rates, Lake Ontario. *Journal of Coastal Research* **13**(4): 1093–1101.

Beetham EP, Kench PS. 2011. Field observations of infragravity waves and their behaviour on rock shore platforms. *Earth Surface Processes and Landforms* **36**(14): 1872–1888.

Benumof BT, Storlazzi CD, Seymour RJ, Griggs GB. 2000. The relationship between incident wave energy and seacliff erosion rates: San Diego County, California. *Journal of Coastal Research* **16**(4): 1162–1178.

Blackmore PA, Hewson PJ. 1984. Experiments on full-scale wave impact pressures. *Coastal Engineering* **8**(4): 331–346.

Bromirski PD. 2001. Vibrations from the "perfect storm". *Geochemistry, Geophysics, Geosystems* **2**: 1030.

Brown EA, Wu CH, Mickelson DM, Edil TB. 2005. Factors controlling rates of bluff recession at two sites on Lake Michigan. *Journal of Great Lakes Research* **31**(3): 306–321.

Budetta P, Galietta G, Santo A. 2000. A methodology for the study of the relation between coastal cliff erosion and the mechanical strength of soils and rock masses. *Engineering Geology* **56**(3): 243–256.

Camfield FE. 1991. Wave forces on wall. *Journal of Waterway, Port, Coastal, and Ocean Engineering* **117**(1): 76–79.

Cartwright N, Baldock TE, Nielsen P, Jeng DS, Tao L. 2006. Swash–aquifer interaction in the vicinity of the water table exit point on a sandy beach. *Journal of Geophysical Research, Oceans* **111**(C9): 1–13.

Castedo R, Murphy W, Lawrence J, Paredes C. 2012. A new process–response coastal recession model of soft rock cliffs. *Geomorphology* **177**: 128–143.

Collins BD, Sitar N. 2008. Processes of coastal bluff erosion in weakly lithified sands, Pacifica, California, USA. *Geomorphology* **97**: 483–501.

Cuomo G, Allsop W, Bruce T, Pearson J. 2010. Breaking wave loads at vertical seawalls and breakwaters. *Coastal Engineering* **57**(4): 424–439.

Cross RH. 1967. Tsunami surge forces. *Journal of Waterways and Harbor Division ASCE* **93**(4): 201–231.

Davidson-Arnott RG, Ollerhead J. 1995. Nearshore erosion on a cohesive shoreline. *Marine Geology* **122**(4): 349–365.

Dickson ME, Pentney R. 2012. Micro-seismic measurements of cliff motion under wave impact and implications for the development of near-horizontal shore platforms. *Geomorphology* **151**: 27–38.

Dickson ME, Ogawa H, Kench PS, Hutchinson A. 2013. Sea-cliff retreat and shore platform widening: steady-state equilibrium? *Earth Surface Processes and Landforms* **38**(9): 1046–1048.

Earlie CS, Young AP, Masselink G, Russell PE. 2015. Coastal cliff ground motions and response to extreme storm waves. *Geophysical Research Letters* **42**: 847–854.

Hackney C, Darby SE, Leyland J. 2013. Modelling the response of soft cliffs to climate change: A statistical, process-response model using accumulated excess energy. *Geomorphology* **187**: 108–121.

Hughes MG, Moseley AS, Baldock TE. 2010. Probability distributions for wave runup on beaches. *Coastal Engineering* **57**(6): 575–584.

Jenkins GM, Watts DG. 1968. Spectral Analysis and Its Applications. Holden Day: San Francisco, CA.

Kamphuis JW. 1987. Recession rate of glacial till bluffs. *Journal of Waterway, Port, Coastal, and Ocean Engineering* **113**(1): 60–73.

Kennedy MP. 1975. Bulletin 200. In Geology of the San Diego Metropolitan Area, Western Area. Sacramento, CA: California Division Mines and Geology.

Kline SW, Adams PN, Limber PW. 2014. The unsteady nature of sea cliff retreat due to mechanical abrasion, failure and comminution feedbacks. *Geomorphology* **219**: 53–67.

Kirk RM, Komar PD, Allen JC, Stephenson WJ. 2000. Shoreline erosion on Lake Hawea, New Zealand, caused by high lake levels and storm-wave runup. *Journal of Coastal Research* **16**: 346–356.

Larson M, Erikson L, Hanson H. 2004. An analytical model to predict dune erosion due to wave impact. *Coastal Engineering* **51**(8): 675–696.

Leighton and Associates. 2003. Del Mar Bluffs Stabilization, Project 2 – Preserving Trackbed Support, Supplemental Geotechnical Evaluation

and Determination of Site Specific Conceptual Repair Alternatives. Manchester: Leighton and Associates.

Lim M, Rosser NJ, Petley DN, Keen M. 2011. Quantifying the controls and influence of tide and wave impacts on coastal rock cliff erosion. *Journal of Coastal Research* **27**(1): 46–56.

Limber PW, Murray AB, Adams PN, Goldstein EB. 2014. Unraveling the dynamics that scale cross-shore headland relief on rocky coastlines: 1. Model development. *Journal of Geophysical Research, Earth Surface* **119**(4): 854–873.

Naylor LA, Kennedy DM, Stephenson WJ. 2014. Synthesis and conclusion to the rock coast geomorphology of the world. *Geological Society, London, Memoirs* **40**(1): 283–286.

Naylor LA, Stephenson WJ, Trenhaile AS. 2010. Rock coast geomorphology: recent advances and future research directions. *Geomorphology* **114**(1): 3–11.

Norman EC, Rosser NJ, Brain MJ, Petley DN, Lim M. 2013. Coastal cliff-top ground motions as proxies for environmental processes. *Journal of Geophysical Research, Oceans* **118**(12): 6807–6823.

Ogawa H. 2012. Observation of wave transformation on a sloping type B shore platform under wind-wave and swell conditions. *Geo-Marine Letters* **33**(1): 1–11.

O'Reilly WC, Guza RT. 1991. Comparison of spectral refraction and refraction-diffraction save models. *Journal of Waterway, Port, Coastal, and Ocean Engineering – ASCE* **117**(3): 199–215.

O'Reilly WC, Guza RT. 1993. A comparison of two spectral wave models in the southern California Bight. *Coastal Engineering* **19**: 263–282.

O'Reilly WC, Guza RT. 1998. Assimilating coastal wave observations in regional swell predictions. Part I: Inverse methods. *Journal of Physical Oceanography* **28**(4): 679–691.

Oumeraci H, Klammer P, Partenscky HW. 1993. Classification of breaking wave loads on vertical structures. *Journal of Waterway, Port, Coastal, and Ocean Engineering* **119**(4): 381–397.

Oumeraci H, Kortenhaus A, Allsop NWH, De Groot MB, Crouch RS, Vrijling JK, Voortman HG. 2001. Probabilistic Design Tools for Vertical Breakwaters. Balkema: Rotterdam; 392 pp.

Pawka SS. 1983. Island shadows in wave directional spectra. *Journal of Geophysical Research* **88**(C4): 2579–2591.

Poppeliers C, Mallinson D. 2015. High-frequency seismic noise generated from breaking shallow water ocean waves and the link to time-variable sea states. *Geophysical Research Letters* **42**(20): 8563–8569.

Raubenheimer B, Guza RT, Elgar S, Kobayashi N. 1995. Swash on a gently sloping beach. *Journal of Geophysical Research, Oceans* **100** (C5): 8751–8760.

Revell DL, Battalio R, Spear B, Ruggiero P, Vandever J. 2011. A methodology for predicting future coastal hazards due to sea-level rise on the California Coast. *Climatic Change* **109**(1): 251–276.

Robinson LA. 1977. Marine erosive processes at the cliff foot. *Marine Geology* **23**(3): 257–271.

Ruggiero P, Komar PD, McDougal WG, Marra JJ, Beach RA. 2001. Wave runup, extreme water levels and the erosion of properties backing beaches. *Journal of Coastal Research* **17**: 407–419.

Sallenger AH, Jr, Krabill W, Brock J, Swift R, Manizade S, Stockdon H. 2002. Sea-cliff erosion as a function of beach changes and extreme wave runup during the 1997–1998 El Niño. *Marine Geology* **187**: 279–297.

Shih SM, Komar PD, Tillotson KJ, McDougal WG, Ruggiero P. 1994. Wave run-up and sea-cliff erosion. In Coastal Engineering 1994 Proceedings, 24th International Conference. American Society of Civil Engineers: Reston, VA; 2170–2184.

Stockdon HF, Holman RA, Howd PA, Sallenger AH. 2006. Empirical parameterization of setup, swash, and runup. *Coastal Engineering* **53**(7): 573–588.

Sunamura T. 1977. A relationship between wave-induced cliff erosion and erosive force of waves. *The Journal of Geology* **85**(5): 613–618.

Sunamura T. 1982. A predictive model for wave-induced cliff erosion, with application to Pacific coasts of Japan. *The Journal of Geology* **90**(2): 167–178.

Sunamura T. 2015. Rocky coast processes: with special reference to the recession of soft rock cliffs. *Proceedings of the Japan Academy, Series B* **91**(9): 481–500.

Stephenson WJ, Kirk RM. 2000. Development of shore platforms on Kaikoura Peninsula, South Island, New Zealand: Part one: the role of waves. *Geomorphology* **32**(1): 21–41.

Swenson MJ, Wu CH, Edil TB, Mickelson DM. 2006. Bluff recession rates and wave impact along the Wisconsin coast of Lake Superior. *Journal of Great Lakes Research* **32**(3): 512–530.

Trenhaile AS. 2000. Modeling the development of wave-cut shore platforms. *Marine Geology* **166**(1): 163–178.

Trenhaile AS. 2011. Predicting the response of hard and soft rock coasts to changes in sea level and wave height. *Climatic Change* **109**(3–4): 599–615.

Vann Jones (née Norman) EC, Rosser NJ, Brain MJ, Petley DN. 2015. Quantifying the environmental controls on erosion of a hard rock cliff. *Marine Geology* **363**: 230–242.

Wilcock PR, Miller DS, Shea RH, Kerkin RT. 1998. Frequency of effective wave activity and the recession of coastal bluffs: Calvert Cliffs. *Maryland. Journal of Coastal Research* **14**(1): 256–268.

Young AP. 2015. Recent deep-seated coastal landsliding at San Onofre State Beach, California. *Geomorphology* **228**: 200–212.

Young AP, Adams PN, O'Reilly WC, Flick RE, Guza RT. 2011a. Coastal cliff ground motions from local ocean swell and infra-gravity waves in southern California. *Journal of Geophysical Research* **116**: C09007, DOI. 10.1029/2011JC007175

Young AP, Guza RT, Adams PN, O'Reilly WC, Flick RE. 2012. Cross-shore decay of cliff top ground motions driven by local ocean swell and infragravity waves. *Journal of Geophysical Research* **117**: C06029. DOI. 10.1029/2012JC007908

Young AP, Guza RT, Dickson ME, O'Reilly WC, Flick RE. 2013. Ground motions on rocky, cliffed, and sandy shorelines generated by ocean waves *Journal of Geophysical Research* **118**: 6590–6602, DOI. 10.1002/2013JC008883

Young AP, Guza RT, Flick RE, O'Reilly WC, Gutierrez R. 2009. Rain, waves, and short-term evolution of composite seacliffs in southern California. *Marine Geology* **267**(1): 1–7.

Young AP, Guza RT, O'Reilly WC, Flick RE, Gutierrez R. 2011b. Short-term retreat statistics of a slowly eroding coastal cliff. *Natural Hazards and Earth System Science* **11**(1): 205–217.